

# Terrestrial Planet Formation from an Annulus

Kevin J. Walsh, Harold F. Levison

*Southwest Research Institute, 1050 Walnut St. Suite 300, Boulder, CO 80302, USA*

`kwalsh@boulder.swri.edu`

## ABSTRACT

It has been shown that some aspects of the terrestrial planets can be explained, particularly the Earth/Mars mass ratio, when they form from a truncated disk with an outer edge near 1.0 au (Hansen 2009). This has been previously modeled starting from an intermediate stage of growth utilizing pre-formed planetary embryos. We present simulations that were designed to test this idea by following the growth process from km-sized objects located between 0.7–1.0 au up to terrestrial planets. The simulations explore initial conditions where the solids in the disk are planetesimals with radii initially between 3 and 300 km, alternately including effects from a dissipating gaseous solar nebula and collisional fragmentation. We use a new Lagrangian code known as LIPAD (Levison et al. 2012), which is a particle-based code that models the fragmentation, accretion and dynamical evolution of a large number of planetesimals, and can model the entire growth process from km-sizes up to planets.

A suite of large ( $\sim$  Mars mass) planetary embryos is complete in only  $\sim 1$  Myr, containing most of the system mass. A quiescent period then persists for 10-20 Myr characterized by slow diffusion of the orbits and continued accretion of the remaining planetesimals. This is interrupted by an instability that leads to embryos crossing orbits and embryo-embryo impacts that eventually produce the final set of planets. While this evolution is different than that found in other works exploring an annulus, the final planetary systems are similar, with roughly the correct number of planets and good Mars-analogs.

*Subject headings:* planets and satellites: terrestrial planets – planets and satellites: formation – planets and satellites: dynamical evolution and stability

## 1. Introduction

An important and challenging issue in understanding terrestrial planet formation are the large differences between Earth and Mars. The two planets are solar system neighbors but are separated by an order of magnitude in mass and accretion age (Nimmo & Kleine 2007; Kleine et al. 2009; Dauphas & Pourmand 2011). Classical models of terrestrial planet formation with initial conditions

that include smooth disks of solid material extending beyond  $\sim 2$  au and that started with a population consisting of both km-scale planetesimals and Moon-to-Mars mass embryos generally fail to capture either of these two constraints (see [Raymond et al. 2009](#) or a review by [Morbiddelli et al. 2012](#)).

Recent works have explored conditions with non-smooth surface density profiles of solids with some successes being found for a truncated disk with an outer edge at or near 1 au ([Hansen 2009](#); [Walsh et al. 2011](#); [Izidoro et al. 2014](#); [Jacobson & Morbidelli 2014](#); [Levison et al. 2015](#)). The altered surface density was found to promote a scattering of Mars-analogs where they then avoid further embryo-embryo impacts and accretion events — essentially starving Mars, keeping it small and ending its accretion much earlier than the Earth.

However, most previous works begin modeling at an intermediate stage of growth - with “planetary embryos” amidst a sea of “planetesimals” - and then truncate the disk or remove mass in certain regions. However, this does not consider the context of how such initial conditions came to be. For example, if solid material never formed beyond 1.0 au, how differently would the initial generation of planetesimals behave as they grew into the planetary embryos? Would there have been diffusion of material off the sharp edges of the mass distribution? We test an end-member case, essentially an initial disk truncation, and test if a disk of planetesimals (diameters of 10s of km), situated between 0.7–1.0 au grow to become good matches for the terrestrial planets.

### 1.1. Previous Work

[Hansen \(2009\)](#) explored a scenario where all solid mass currently in the inner solar system ( $2 M_{\oplus}$ ) was initially between 0.7–1.0 au, and all of it in 400 similar sized objects (each were  $2.98 \times 10^{22}$  kg, or  $\sim 1000$  km radius) with no gas effects. These conditions succeeded in producing a good Earth/Mars mass ratio consistently as embryos were scattered off the edge of the annulus early and avoided further growth near 1.5 au. The accretion timescales for Mars-analogs were fast, largely on order of the estimated timescales from cosmochemical studies between 2-10 Myr ([Nimmo & Kleine 2007](#); [Dauphas & Pourmand 2011](#)). However, the Earth-analogs also formed rapidly, on roughly similar timescales, which is much faster than cosmochemical expectations of 30-100 Myr ([Kleine et al. 2004, 2009](#)).

Seeking a mechanism to truncate a disk of solid material, [Walsh et al. \(2011\)](#) invoked the inward-then-outward migration of the Jupiter (where the [Walsh et al. \(2011\)](#) migration of Jupiter is referred to as the “Grand Tack”). This migration was constrained by the need to produce a disk with a truncation at 1.0 au, similar to that of [Hansen \(2009\)](#). The initial conditions included 1/4 to 1/2 Mars mass planetary embryos in a sea of thousands of planetesimals. While these initial conditions were similar to [O’Brien et al. \(2006\)](#) the dynamical effects of Jupiter migrating was a powerful effect and pushed embryos onto crossing orbits. The final planetary systems in this work had a similar mass-semimajor axis distribution as found in [Hansen \(2009\)](#) and later work by

O’Brien et al. (2014) found similar accretion timescales.

Jacobson & Morbidelli (2014) investigated the outcomes for “Grand Tack” scenarios, where the bi-modal mass distribution was altered. Here, correlations were found such that increasing the mass ratio of embryos to planetesimals leads to longer accretion timescales, but also more dynamically excited final systems of planets. Largely, the radial mass distribution (RMC) of the final planets was unchanged for the wide range of parameters explored.

Nebular effects have also been proposed as means to change the surface density profile of the gas disk. Ionization in the gas-disk could lead to regions with very different viscosity creating local mass distribution minimums at the boundaries (Jin et al. 2008). Izidoro et al. (2014) used this as motivation to study planet formation in numerous scenarios with depletions of solid material in annular regions beyond 1 au. For deep depletions of material similar edge effects were found as in Hansen (2009) and Walsh et al. (2011).

Finally, Levison et al. (2015) explored the growth of planets directly from cm-sized “pebbles”. While this work was not designed explicitly to generate an annulus, the accretion efficiency for pebbles (where “pebbles” refer to the direct accretion of cm or small particles) is strongly dependent on both the size of the seed body (embryo or planetesimal) and also the stopping time of the rapidly drifting pebbles. Thus Levison et al. (2015) finds for some initial conditions the rapid growth of embryos inside of  $\sim 1.0$  au with minimal growth at further distances in the inner solar system – essentially generating an annulus of very large planetary embryos.

While these works have studied formation from an Annulus in different ways they all started modeling at an intermediate stage of growth (note that Levison et al. (2015) relied on an entirely different mode of accretion). The most numerically tractable point for commencing a model is after the bi-modal mass distribution is established during “Oligarchic growth”, where after a few to ten million years there may no longer be a gas disk, and there are only tens of embryos amidst a sea of planetesimals. To allow a very large number of planetesimals (thousands), the models typically do not consider gravitational interactions between planetesimals, but the embryos (tens of bodies typically) interact with each other and the planetesimals. As discussed above there are variations on these initial conditions, but nearly all are founded in this initial bi-modal distribution of mass.

Similarly, most studies assume that when two bodies collide they merge perfectly, conserving momentum and mass. This is caused by the numerical problem of introducing new particles into the simulation by way of a collisional fragmentation event and the subsequent computational risk of large, and increasing,  $N$ . While various works have included aspects of fragmentation at different times (see Leinhardt et al. 2009; Kokubo & Genda 2010; Chambers 2013; Carter et al. 2015), only a few models have approached planetesimal to planet simulations (see Kenyon & Bromley 2006; Morishima 2015).

Finally, most of the works starting in Oligarchic growth phases assume the absence of any gas effects. This is partly due to the expected lifetime of the gaseous solar nebula (2-10 Myr) being similar to the expected times to reach the Oligarchic growth stages. While not computationally

difficult to include, the typical absence of gas effects is also partly due to the uncertainties in precisely when and how the gaseous solar nebula dissipated – whether it was a slow loss of mass, or inside-out or outside-in dispersal. However, we will show that in the simple case of an exponential decay of the nebula, even a very small fraction of the original solar nebula can strongly affect the outcome of the models by stabilizing the system for long periods of time.

## 1.2. This work

Most previous works’ initial conditions include planetary embryos, and thus imply significant previous growth and evolution *before* the various truncation/depletion mechanisms happen. None start with an annulus of planetesimals, nor do any constrain how early or late in the stages of growth of the disk that such truncation mechanisms could successfully operate (technically, [Levison et al. \(2015\)](#) starts with planetesimals, but studies a very different growth process).

Here, the question we are trying to answer requires a complete simulation from planetesimals to planets, and thus re-thinking both the initial conditions and also the gas effects requires including particle fragmentation. Specifically, regarding a disk truncation or annulus as a way to address the “small Mars” problem, starting with a bi-modal mass distribution implies previous growth — the embryos have already grown. However, this would assume simple static growth within an annulus not allowing for diffusion of bodies or drift from drag forces.

Thus, this test is simple, but relevant to the concept of forming the Earth/Mars mass ratio due to substantial changes to the mass distribution of the solid material in the disk, and may point to required timing or truncation mechanisms to satisfy constraints. We will include fragmentation throughout the simulations and will include a constantly decaying gas disk and all of its effects on the simulation. Note that this is the first in a series of papers exploring the growth of planetesimals to planets, and so related studies will follow.

## 2. Methods

To model the accretion from planetesimals to planets we use the code LIPAD, which stands for Lagrangian Integrator for Planetary Accretion and Dynamics ([Levison et al. 2012](#)). This code models the fragmentation and accretion of a suite of particles, while also modeling the dynamics of the system. This is necessary for this work as it allows for the wholesale redistribution of mass throughout the system unlike many collisional codes.

We describe two suites of simulations. In the first the primary variable is the initial planetesimal size, with some tests without fragmentation and a set of simulations with no gas effects. These are all referred to as the “LIPAD suite” of simulations, which are distinct from a set of “Hansen” simulations that re-created the initial conditions and simulation techniques of the Hansen (2009)

work. These also tested the impact of gas effects and the results are described in the Conclusion.

### 2.1. LIPAD: planetesimals to planets

LIPAD is built on top of the  $N$ -body algorithms known as the Wisdom-Holman Mappings (WHM; Wisdom & Holman 1991), and treats close encounters between bodies using the algorithms of SyMBA (Duncan et al. 1998). LIPAD utilizes “tracer” particles that each represent a significant total mass for calculating the gravitational evolution of the system. Each tracer is given a radius  $s$ , so that during the simulation it represents a swarm of particles each of radius  $s$ , where the sum of their mass equals the mass of the tracer itself. Collisional probabilities are calculated for each tracer as a function of its size  $s$  and the total mass, sizes and orbits of its neighbors. The dynamics of each tracer is modeled with direct gravity calculations as well as other dynamical effects (dynamical friction, viscous stirring), where many calculations depend on the particle’s radius  $s$  and the masses, sizes and orbits of its neighbors.

When a collision between tracers occurs the Benz & Asphaug (1999) fragmentation law is used to determine the outcome. This determines the expected size distribution of fragments, and a radius  $s$  is chosen from the distribution for each tracer involved. To represent the full size distribution of the system requires the inclusion of many tracer particles, each with different sizes  $s$ . This algorithm has been found to match standard collisional evolution codes due to the high number of collisions and using a high enough particle resolution ( $\sim$  thousand particles per au) so that collisional environments can vary regionally (see Levison et al. 2012).

When particles break, there is a minimum size that is allowable from the collisional cascade - `rfmin`. This lower limit is important for computation times, as smaller sizes mean more collisions to calculate. However, the physics of very small particles can be important in the evolution of a planetary system as aerodynamic drag drift rates increase with decreasing size down to meter-sizes and radiation effects start to increase below cm-sizes. Here, the smallest tracer size allowed was 1 km. Tracers below that size remain in the simulation but stop interacting with other tracer particles in the collisional cascade, but still interact with larger planetary embryos with the possibility of being accreted or ejected from the system due to gravitational interactions.

At the small end of the size distribution, tracers below 1 km in size are treated as “dust”, whereby they experience Poynting Robertson drag with a magnitude for a 30 micron particle. This simplification saves computational time, as resolving the size distribution to micron, or even meter, sizes is numerically expensive. We tested the sensitivity of this parameter, the smallest allowable size, for a case with and without gas, where tracers could be as small as 1 m. We found more mass loss due to collisional grinding that was roughly  $\sim 10\%$  greater (turning to “dust” and being removed by PR drag), for the simulation setting with the 1 m smallest tracer size. The size frequency distributions were not substantially altered. Combined, the systematic, and relatively small, extra mass loss, combined with minimal changes in size distributions support our

computationally expedient choice of 1 km smallest size. This difference has been found to be much more important in full-disk simulations (0.7–3.0 au) where the production of “dust” can happen in very different regions of the disk at very different timescales, and that work will be presented in an upcoming publication.

At the large end of the size distribution, tracers are promoted to embryos at  $R = 874$  km, at which point their mass can increase and their collisional evolution changes. They now revert to “perfect merging” when colliding with other embryos, while collisions with tracers can modify the tracer properties as described above, or result in a merger with the embryo.

Numerous gas affects are included in each simulation (see [Levison et al. 2012](#) for discussions). There is a gas disk with density  $1.4 \times 10^{-9}$  g cm $^{-3}$  at 1 au. The disk density decays from this value with a 2 Myr e-folding lifetime. While present, the gas imposes aerodynamic drag on the particles as a function of their radius  $s$ , and also Type-I eccentricity damping, which acts exclusively on the planetary embryos (see [Levison et al. 2012](#) for formulations). The timescale and decay profile of the gaseous nebula can have profound effects on the outcome of these models - for the sake of simplicity while we explore these basic questions with a new code we will use either no gas or this singular decay timescale in this work.

## 2.2. The LIPAD suite

The simulations all utilize 2612 tracer particles with randomly generated semimajor axes between 0.7–1.0 au that follow a  $1/r$  surface density distribution. The primary variable examined was the average initial size of the tracer particles. Three values were tested in different subsets of simulations, where in each the particle initial radius distribution was a gaussian centered on  $R_{\text{init}} = 3$  km, 30 km and 300 km, with dispersions equal to 10% in each case.

Particles had a density of 3 g cm $^{-3}$  throughout, and each tracer represented a mass of  $9.35 \times 10^{-4}$   $M_{\oplus}$  for a total of 2.44  $M_{\oplus}$  in the system. As growth occurs tracer particles transition to sub-embryos when they reach a radius,  $\sim 760$  km and they become full-embryos at a radius of  $\sim 3400$  km (see [Levison et al. 2012](#) for more details on the treatment of sub-embryos and embryos).

The initial eccentricity and inclination distributions were Rayleigh distributions. For the  $R_{\text{init}} = 30$  km and 300 km the distribution was centered on  $e = 5 \times 10^{-5}$  and  $i = 0.002^\circ$ , while for  $R_{\text{init}} = 3$  km it was centered on  $e = 5 \times 10^{-6}$  and  $i = 0.0002^\circ$ . For each initial planetesimal size, four simulations were run for each case with different randomly generated initial conditions. The timestep was 0.025 yr ( $\sim 9$  days), and the simulations were run for 115 Myr, which take over a month computation time running on 4-6 processors. Particles that attained a heliocentric distance smaller than 0.045 au were removed from the simulation, as were those that had a distance beyond 2000 au.

### 2.3. The Hansen Suite

The simulations of [Hansen \(2009\)](#) provide an excellent (and fast) testbed to explore the powerful effects that the gas disk can have the evolution of a disk of solids. The simulations contain  $2 M_{\oplus}$  of material split between 400 bodies on orbits randomly situated with semimajor axes between 0.7–1.0 au. These  $R_{\text{init}}=1070$  km planetary embryos were  $0.05 M_{\oplus}$  each and were randomly distributed between 0.7–1.0 au with initial eccentricity and inclinations as Rayleigh distributions centered on  $e = 0.0004$  and  $i = 0.01^{\circ}$ .

LIPAD was configured to allow perfect merging only, with no fragmentation – essentially making it a classical SyMBA or MERCURY simulation. There were no gas effects in one suite of four simulations, which essentially mimic the [Hansen \(2009\)](#) work. In the other set of simulations a gas disk with the properties described above was included. This disk decay time and initial density was the same as before: 2 Myr and  $1.4 \times 10^{-9} \text{ gm cm}^{-3}$  at 1 au respectively.

## 3. Results

The focus of this study are the simulations described in the LIPAD suite above. For each initial  $R_{\text{init}}$ , which varied by two orders of magnitude, there were four separate simulations performed. There were also tests carried out with no fragmentation and no gas, and for these the  $R_{\text{init}}=30$  km was used. Thus we explore a singular parameter over a wide range of values  $R_{\text{init}}$  and two others for a fiducial value of  $R_{\text{init}}$ , and aim to have statistics based on running each multiple times.

### 3.1. Evolution and Growth of Planets in LIPAD

The evolution of the annulus of planetesimals followed familiar growth patterns that have been explored extensively in the literature progressing through two stages of growth in the first  $\sim 10$  Myr, where in [Fig 1](#) each example simulation is in the midst of Runaway growth by 100, 50 and 10 Kyr for  $R_{\text{init}}=300$ , 30 and 3 km respectively. The annulus quickly entered Runaway growth, where the mass ratio between the largest body and the small bodies is increasing with time (see [Fig. 2](#)).

For each  $R_{\text{init}}$  the growth of the largest bodies suggests that they have reached Oligarchic growth by  $\sim 1$  Myr (see mass of the largest body over time in [Fig. 2](#)), where Oligarchic growth is typically considered to be begin when the stirring power of the large bodies exceeds that of the small bodies ([Ida & Makino 1993](#)). Therefore the size at which this transition happens has a functional dependence on the initial planetesimal size - the size of the small bodies. In terms of radius, for the three sets of initial conditions  $R_{\text{init}}=300$ , 30 and 3 km this transition should take place when bodies grow to 440 km, 110 km and 28 km ([Ormel & Dullemond... 2010](#); [Thommes et al. 2003](#)). Oligarchic growth continues until embryo-embryo collisions begin and the onset of instabilities begins closer to  $\sim 10$  Myr (see [Sec. 3.3](#) below for characterization of instabilities and the onset of



the Giant Impact stage).

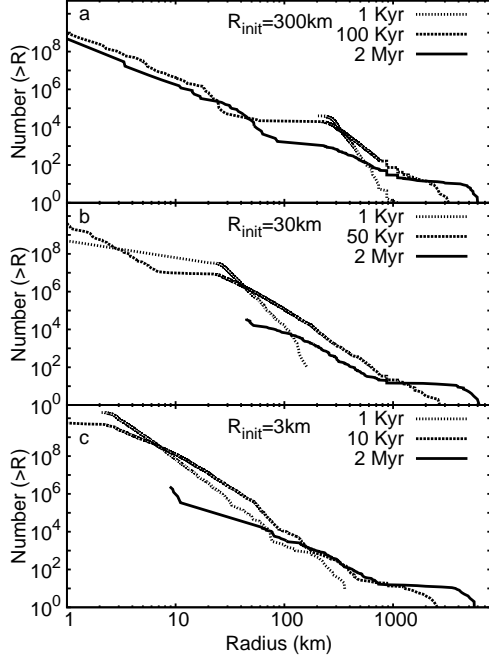


Fig. 1.— The number of particles with radius of  $N(> R)$  as a function of the radius of the particles  $R$  for one representative simulation from each  $R_{\text{init}}$ . Pane (a) is for the simulations with  $R_{\text{init}} = 300$  km, (b) for  $R_{\text{init}} = 30$  km and (c) for  $R_{\text{init}} = 3$  km. Note that each pane plots slightly different times. The  $R_{\text{init}} = 3$  km reaches “runaway” growth much earlier than for the larger initial radius runs, but all three look similar at 2 Myr. Note, this is a not a true size frequency distribution, rather the representative sizes of the tracer particles in the simulation.

The spacing of the planetary embryos (where anything larger than 1/70th the mass of the Earth is included for this calculation as an “embryo”) is similar for each set of initial conditions (Fig. 3). At 1 Myr, where the simulations had on average 12 embryos each, the distribution of spacing in terms of mutual Hill Spheres peaks around 6 for each  $R_{\text{init}}$ . The spacing, in terms of semimajor axis, slowly increases with time for all cases, until  $\sim 10$  Myr, at which time the spacing starts to grow substantially as simulations start to enter the Giant Impact stage of growth. This evolution is in line with the expectations and previous results for the spacing of embryos during the Oligarchic growth stage (Kokubo & Ida 1998).

Mass can be lost from the simulations due to the inclusion of fragmentation, gas drag effects and Poynting Robertson (PR) drag. In Figure 4 a clear trend for more surviving final mass in embryos is found for increasing  $R_{\text{init}}$  with only 1.6, 2.0 and 2.2  $M_{\oplus}$  remaining for 3, 30 and 300 km respectively (where the embryo mass is a proxy for system mass as planetesimal mass approaches zero in all cases). This is due to more efficient grinding at smaller sizes. The smallest  $R_{\text{init}}$  shows



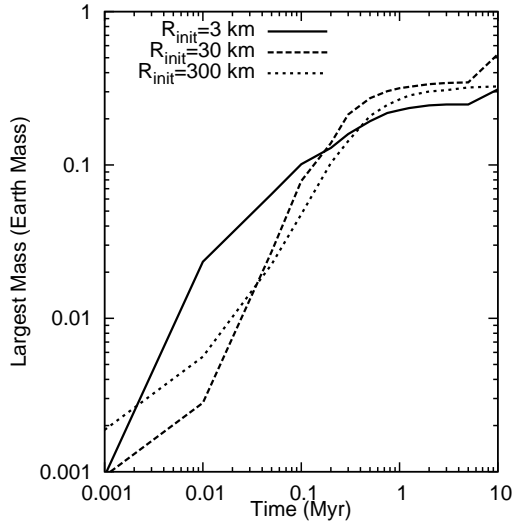


Fig. 2.— Growth of the largest bodies in representative simulations for each tested  $R_{\text{init}}$ , showing the mass of the largest body in Earth masses as a function of time.

the fastest growth in the first 100,000 years and the earliest production of embryos, which would stir the neighboring disk and promote collisional grinding earlier. The case with no gas disk shows substantial mass loss, with over half of the mass lost from the system, due to the dynamical excitement early in the disk evolution when there were still many small planetesimals to grind away.

### 3.2. The Planets

In this work we consider “Planets” to be anything over 1/30th the mass of the Earth (unlike many classical works we grow our embryos and so we selected  $\sim 1/2$  Mercury mass to cover the entire range of planetary mass). We define a Mars-analog as any planet that has a semimajor axis between 1.2 and 2.0 au. Therefore some simulations may have multiple Mars-analogs (though this is rare in these simulations - and we attempt to indicate the cases and discuss further individually).

#### 3.2.1. Bulk properties

The properties of the formed planetary systems are listed in Table 1. The average number of planets formed for each suite of 4 simulations was 3.5, 3.25 and 5.25 for  $R_{\text{init}} = 3, 30$  and 300 km respectively, and 3.75 for  $R_{\text{init}} = 30$  km with no gas. The total mass remaining in the planetary systems decreases with  $R_{\text{init}}$ , averaging over  $2 M_{\oplus}$  for  $R_{\text{init}} = 300$  km, and  $1.26 M_{\oplus}$  for  $R_{\text{init}} = 3$  km. This is due the affects of collisional grinding as mentioned above. For the case with no gas

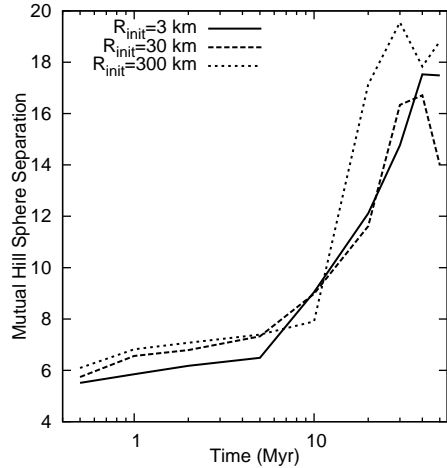


Fig. 3.— Embryos spacings in units of mutual Hill Spheres, for all of the simulations with  $R_{\text{init}} = 3, 30$  and  $300$  km, as a function of time.

the grinding was more severe, and the mass loss was due to grinding to very small sizes and drag removing particles — these cases ended with below  $1 M_{\oplus}$  of planets.

One can rely on some typical metrics to assess the mass distribution and orbital excitement compared to the current system of Terrestrial Planets and previous modeling efforts. To measure the mass distribution, we use the radial mass concentration statistic (RMC), defined as

$$RMC = \max \left( \frac{\sum M_j}{\sum M_j [\log_{10}(a/a_j)]^2} \right), \quad (1)$$

where  $M_j$  and  $a_j$  are the mass and semimajor axis of planet  $j$  (Chambers 2001). The function in brackets is calculated for a range of  $a$  (0.7–1.2 au) in the terrestrial planet region with the maximum value being selected (following the prescription of Chambers 2001). This metric returns infinity for a single planet system, and decreases towards zero as mass gets spread out across a range of semimajor axes. The current value for the solar system is 89.9. This value exceeds all outcomes for  $R_{\text{init}} = 30$  and  $300$  km, where their low values point to a wider distribution of masses (see Table 1). For example for  $R_{\text{init}} = 300$  km, run (003), the RMC is skewed low due to the presence of a large ( $0.57 M_{\oplus}$ ) and distant ( $a = 1.7$  au) Mars-analog. The simulations for  $R_{\text{init}} = 3$  km and the  $R_{\text{init}} = 30$  km with no gas typically exceeded the solar system RMC – sometimes due to a small number of centrally (near 1 au) located planets (as in one case for  $R_{\text{init}} = 3$  km that produced only 2 planets).

A common metric used to measure the dynamical excitation of a planetary system is the angular momentum deficit (AMD; Laskar 1997):

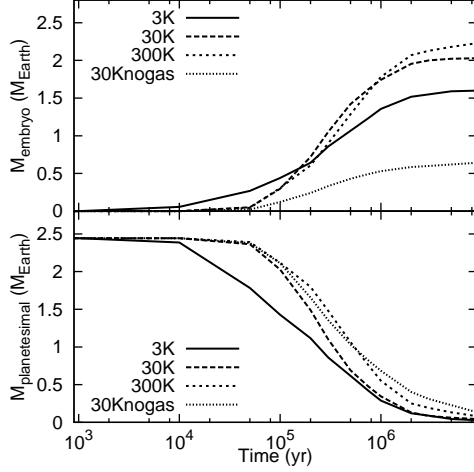


Fig. 4.— The (upper panel) total mass of embryos in units of Earth Masses as a function of time for three nominal simulations at each  $R_{\text{init}}$ , and also for the  $R_{\text{init}}=30$  km case with no gas. The (bottom panel) total planetesimal mass as a function of time for the same simulations.

$$AMD = \frac{\sum_j M_j \sqrt{a_j} \left(1 - \cos(i_j) \sqrt{1 - e_j^2}\right)}{\sum_j M_j \sqrt{a_j}}, \quad (2)$$

where  $M_j$  and  $a_j$  are again the mass and semimajor axis, while  $i_j$  and  $e_j$  are the inclination and eccentricity of each planet  $j$ . The current solar system has an  $AMD = 0.0014$ . All of the  $R_{\text{init}}=3$  and 30 km simulations had final AMD values exceeding the solar system value, typically by a factor of 2–10. The two  $R_{\text{init}}=300$  km cases with similar or lower AMD values were the two cases with 7 planets. Generally, as will be discussed below, the systems had depleted nearly all planetesimals before having any major orbital instability, leaving behind insufficient masses of planetesimals to significantly damp the orbits of the final planets. Note, that as will be discussed in the Conclusions below, the way that this code handles the fragmentation of embryos may change the amount of damping provided by planetesimals produced *during* the final few giant impacts.

Ten of the twelve baseline simulations (all the cases with gas described so far) produced a Mars-analog, and 13 total Mars-analogs were produced - where a Mars-analog is any embryo between 1.2 and 2.0 au ( $R_{\text{init}}=300$  cases (001) and (004) each had two Mars-analogs, along with  $R_{\text{init}}=3$  km (003)). The Mars-analogs were on average  $0.16 M_{\oplus}$  and located at 1.56 au - these simulations produce reasonable Mars-analogs. The low RMC values values discussed above are therefore not due to Mars-analogs being large, but rather due to the depressed masses of, or absence of, Earth- and Venus-analogs. This is notable in the figures of each set of simulations mass compared with the semimajor axis, where planets at 1.0 au are often only half the mass of the Earth (see Figures 5, 6, 7).

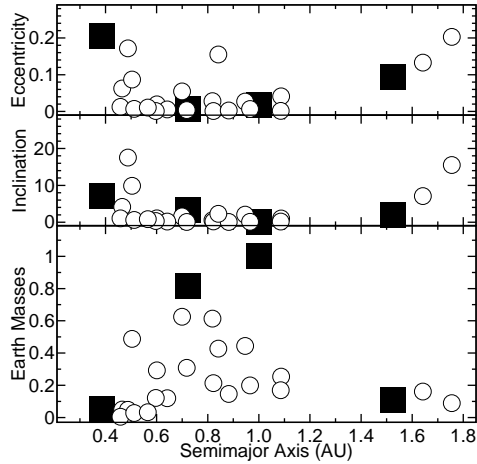


Fig. 5.— The final planets, after 115Myr of evolution, for  $R_{\text{init}} = 3$  km. Plotted are the (top) eccentricity, (middle) inclination in degrees and (bottom) mass as a function of semimajor axis. The large black squares are the values for Mercury, Venus, Earth and Mars, while the open circles are the simulation outcomes.

### 3.3. Instabilities and Last Giant Impacts

Many of the simulations showed long periods of quiescent behavior, followed by a short interval of crossing orbits, embryo-embryo impacts and a rapid decrease in the number of embryos or planets. These instabilities were tracked using the metric of recording the beginning of a 1 Myr interval where at least two embryo-embryo collisions occurred. While inexact, this metric provides a quick look at when a system evolves from a dynamically cold suite of many planets and reduces its numbers (this metric,  $t_{\text{inst}}$  is reported in the table of results Table 1).

The similarity in instability times was somewhat surprising, where, for example in the  $R_{\text{init}} = 300$  km cases, all four simulations had at least one instability between 10.5–13.7 Myr. The 12 baseline test cases all had instabilities between 8.4–19.8 Myr. There is no apparent connection between any of the studied outcomes (number of planets, Mars-analogs etc.) and the existence or timing of the instabilities.

The last giant impacts,  $t_{\text{Limp}}$ , were determined by last impact that included two planetary embryos. The timing of these were not clearly correlated with  $R_{\text{init}}$ , or the other instability times. Each suite of  $R_{\text{init}}$  had some relatively early last impacts,  $< 25$  Myr, and some relatively late impacts  $> 75$  Myr.

The clearest correlation is the rise of AMD values with the late decrease of number of planets in each simulation. Plotted in Fig. 8 is the evolution of the 4 different  $R_{\text{init}} = 30$  km cases evolution of number of planets and the corresponding AMD values as a function of time. The AMD values remain relatively low beyond 10 Myr (with occasional spikes), and only rise to their final elevated

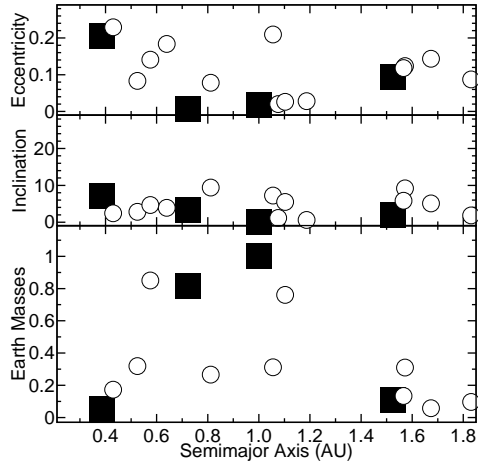


Fig. 6.— The final planets, after 115Myr of evolution, for  $R_{\text{init}} = 30$  km. Plotted are the (top) eccentricity, (middle) inclination in degrees and (bottom) mass as a function of semimajor axis. The large black squares are the values for Mercury, Venus, Earth and Mars, while the open circles are the simulation outcomes.

levels at the beginning of the final instability (as shown by the drop in  $N_{\text{pl}}$  in the top pane). The once dynamically cold systems, with low AMD, get dynamically excited, and start losing planets to giant impacts, until their final planetary suite is reached.

The instability times found here, range from 8 Myr to 18 Myr, which for the gas disk dissipating with a 2 Myr e-folding time, finds that between 1.8% and 0.12% of the initial gas density is present. Previous works focusing on orbital stability of systems as a function of their Hill spacing and gas disk surface density find that less than 0.1% of the nebular gas (in terms of MMSN) must remain to find instabilities for systems with typical Hill spacing ( $\sim 10$  Hill radii) (Iwasaki et al. 2001; Kominami & Ida 2002). Our findings are in line with this previous work and together point to an important dependence on a system’s initial instability on a very small fraction of an initial gaseous nebula.

Another way of interpreting this behavior is that there are, in affect, two generations of planets. The first is generated from Oligarchic growth, where the embryos reach a dynamically stable configuration due to continued damping effects of the gas and also due to the ability for the annulus to diffuse outward. Then the passage into the Giant Impact phase is sudden and only begins 10’s Myr later.

### 3.4. The effect of the Gas Disk and Fragmentation

The gas disk plays a large role in the outcome of these simulations. The damping provides an environment for rapid growth of embryos and diffusion in semimajor axis without crossing orbits

R <sub>init</sub> (run #)	N <sub>planets</sub>	M <sub>tot</sub>	AMD	RMC	M <sub>Larg</sub> (M <sub>⊕</sub> )	M <sub>M</sub> (M <sub>⊕</sub> )	a <sub>M</sub> (au)	t <sub>Limp</sub>	t <sub>inst</sub>
3 km (001)	4	1.43	0.00252	61.8	0.74	0.11	1.47	34.1	11.0
3 km (002)	4	1.08	0.00914	94.7	0.51			20.8	14.0,16.3
3 km (003)	4	1.24	0.01274	59.1	0.84	0.14	1.27	28.6	14.4
3 km (004)	2	1.27	0.00564	109.7	0.79			75.4	19.8
Average	3.5	1.26	0.00751	80.6	0.72	0.13	1.37	39.7	14.8
30 km (001)	3	1.82	0.02161	42.9	1.20	0.31	1.57	86.4	8.4,36.6
30 km (002)	3	1.57	0.00292	49.2	1.34	0.06	1.67	29.7	12.2,23.6
30 km (003)	3	1.75	0.00209	56.2	1.29	0.13	1.57	24.3	16.6
30 km (004)	4	1.97	0.00939	44.3	0.85	0.10	1.83	53.5	8.6,50.9
Average	3.25	1.78	0.00900	36.9	1.17	0.15	1.66	48.5	11.5
300 km (001)	7	2.22	0.00101	40.4	0.85	0.31	1.21	13.6	10.5,11.9
300 km (002)	3	2.06	0.00665	36.8	1.44	0.14	1.80	104.6	11.6,13.3
300 km (003)	4	1.99	0.01643	20.6	1.00	0.57	1.70	78.8	11.7, 13.0
300 km (004)	7	2.23	0.00065	49.5	0.55	0.18	1.30	16.8	13.7
Average	5.25	2.13	0.00619	36.8	0.96	0.30	1.43	53.5	11.9
30 km no gas (001)	5	0.67	0.00089	162.4	0.29			21.8	20.2
30 km no gas (002)	3	0.62	0.00821	94.7	0.35			71.5	
30 km no gas (003)	3	0.61	0.00707	71.9	0.37	0.04	1.55	101.2	
30 km no gas (004)	4	0.63	0.00168	120.2	0.26	0.02	1.38	10.9	
Average	3.75	0.63	0.00446	112.3	0.32	0.03	1.47	51.4	20.2
30 km no Frag (001)	3	1.82	0.02004	39.1	1.16	0.42	1.24	56.9	18.5
1070 km no Frag no gas (001)	6	1.96	0.00740	66.0	0.88	0.04	1.85	12.5	1.2,4.0,8.9,10.4
1070 km no Frag no gas (002)	6	1.90	0.01758	32.7	0.86	0.07	1.82	70.0	1.3,6.1,8.1
1070 km no Frag no gas (003)	8	1.88	0.00899	45.8	0.94	0.23	1.58	101.3	1.0, 3.9
1070 km no Frag no gas (004)	6	1.93	0.00526	78.0	0.91	0.04	1.66	3.6	1.0,11.5
Average	6.5	1.91	0.00981	55.6	0.90	0.10	1.73	46.9	1.1
1070 km no Frag with gas (001)	4	1.99	0.04572	27.7	0.86	0.31	1.82	104.3	17.1
1070 km no Frag with gas (002)	5	1.99	0.01689	43.2	0.98	0.38	1.38	113.5	92.8
1070 km no Frag with gas (003)	4	1.99	0.01231	41.6	1.03	0.19	1.43	27.1	13.3,17.5
1070 km no Frag with gas (004)	3	1.87	0.01389	47.5	0.95	0.53	1.24	40.8	
Average	4	1.96	0.0222	40.0	0.96	0.35	1.47	71.4	41.1

Table 1: Total mass of planets  $M_{\text{tot}}$ , and the mass of the largest planet in the system,  $M_{\text{Larg}}$ , at 115 Myr. Mass of Mars analogs ( $M_{\text{M}}$ ; if  $1.2 < a < 2.0$ ) and their semimajor axis at completion ( $a_{\text{M}}$ ). The time of the last embryo-embryo impacts,  $t_{\text{Limp}}$ , where an embryo is considered if it is  $1/30 M_{\oplus}$ . The time of any major instabilities ( $t_{\text{inst}}$ ) that result in at least two planet-planet mergers within 1 Myr. Note that 3 km run 003 had a  $0.04 M_{\oplus}$  at 1.62 au.

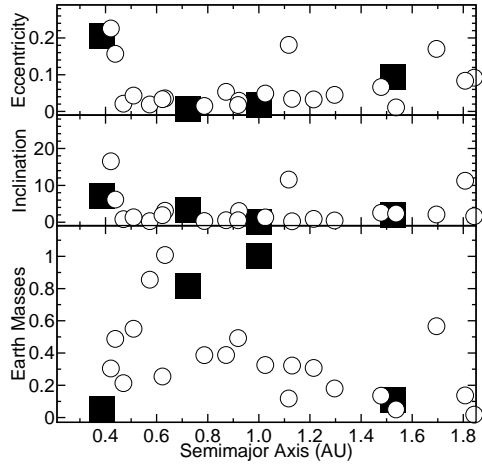


Fig. 7.— The final planets, after 115Myr of evolution, for  $R_{\text{init}}=300$  km. Plotted are the (top) eccentricity, (middle) inclination in degrees and (bottom) mass as a function of semimajor axis. The large black squares are the values for Mercury, Venus, Earth and Mars, while the open circles are the simulation outcomes.

(see Fig. 9). The evolution for the suite of cases run with no gas disk is starkly different than that found for all cases tested with the gas disk discussed above (see Fig. 10).

However, the final systems are, in terms of number of planets and relative distribution of remaining mass, not vastly different than the  $R_{\text{init}}=30$  km simulations with gas. In fact, as will be discussed at length in the Conclusion below, and explored with more test cases, these point to the curious scenario where very different evolutionary paths of two systems reach a similar end state. Figure 11 shows the evolution for a case with gas and case without gas in terms of their number of planets and AMD. Both reach 3 planets and have similar final AMD, but they do so on very different timescales and with a vastly different evolution of the system AMD.

While the effects of the gaseous solar nebula were extreme, the effects of fragmentation were less obvious. To test the effects of collisional evolution on the outcome of the simulations a test was run where particles were allowed to grow, but not fragment, during collisions. The  $R_{\text{init}}$  tested was 30 km, and the evolution was qualitatively similar to that found for the model with fragmentation (see Fig. 12). The clear difference was the total mass in the system, whereby without fragmentation all of the mass stayed in the system and was accreted by the system of embryos (see Fig. 13). For nominal ordered growth in the presence of a long-lasting disk (Myr timescales), the effects of the collisional cascade are not critical – an external source of dust to damp orbits, or a mechanism for dynamic excitation, would be needed to drastically alter the outcomes.



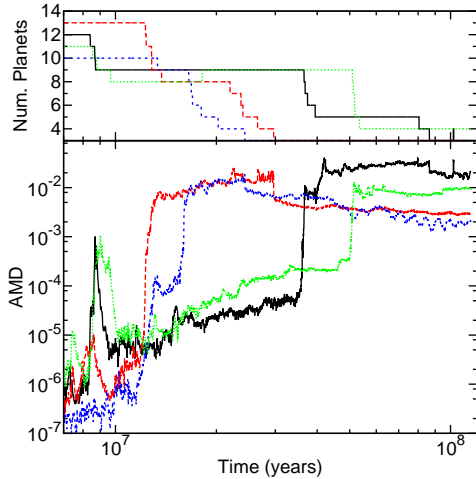


Fig. 8.— The (top) decrease in number of planets in simulations correlated with the (bottom) calculated AMD values as a function of time. This shows all four simulations for the  $R_{\text{init}}=30$  km case.

### 3.5. Comparison with the Hansen suite

Using the various metrics explored above we find that the final planetary system outcomes from these suites of simulations produce adequate matches of the solar system. On average the number of planets is slightly too low and the orbits are too excited. However, Mars-analogs are regularly reproduced, though the mass-semimajor axis distribution (see the RMC metric for the  $R_{\text{init}}=30$  and 300 km cases) suggests that the Earth-analogs are too small and the systems are a bit too spread out. However, for the nominal case of  $R_{\text{init}}=30$  km the systems are reasonable matches.

This is surprising because the evolution of the  $R_{\text{init}}=30$  km systems is decidedly different than the evolution of the successful systems in [Hansen \(2009\)](#). To highlight and explore this further we ran a small series of simulations designed to mimic very directly (and quickly) the original [Hansen \(2009\)](#) simulations with and without gas using LIPAD but without including fragmentation of the tracer particles (just 400 interacting planetary embryos - this is the “Hansen Suite” described above).

The evolution is very different (see Figure 14 left pane) for the simulation using a gas-disk (2 Myr e-folding time). After about  $\sim 1$  Myr there are a small number of embryos, well spaced, and dynamically cold. Meanwhile, for the simulations with no gas the system is very dynamically excited by 1 Myr (see Figure 14 right pane), and the size distribution is not bi-modal, instead having a few embryos as large as found in the gas-disk case and a range of smaller embryos.

The final systems from this test are remarkably similar to each other (see Fig. 15). The cases with the 2-Myr gas disk evolve into an Oligarchic bi-modal distribution with nearly all mass in embryos, and only later evolve through an instability to break from a cold system of many planets

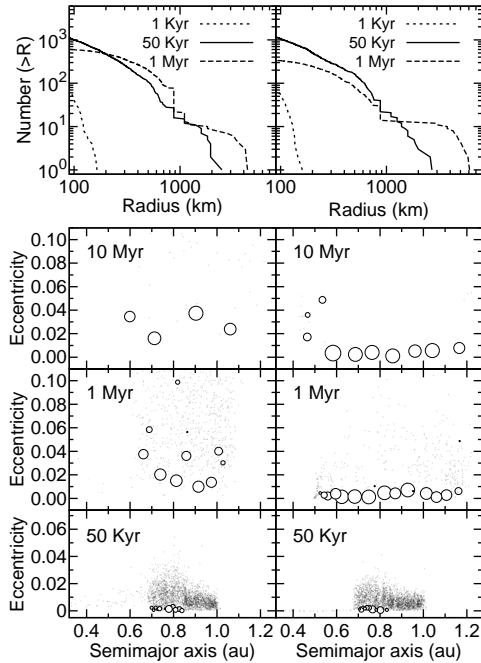


Fig. 9.— The top two panes show the size distribution in each of the simulations with no gas (left) and those with gas (right) at three different times. The bottom panes show the evolution of these two simulations in terms of eccentricity and semi-major axis (au).

to reach a final system observed. Meanwhile the simulations with no gas stay excited with regular embryo-embryo impacts and maintain significant dynamical excitement throughout.

This divergent evolution with similar final results mirrors that seen in the LIPAD suite of simulation that behaved similar to these tests run with gas effects. Despite evolving through a long quiescent period, and having two generations of planets, the final systems are similar.

#### 4. Conclusions

The intent of this study was to explore whether there were limits on building good Mars-analogs and Earth/Mars mass ratios from a truncated disk or annulus. The end-member case of an annulus of km-sized planetesimals was modeled including gas and fragmentation effects, and found in most cases to produce adequate matches to the observed terrestrial planets, including Mars analogs.

However, as explored above, while these may produce similar final systems of planets as in the original [Hansen \(2009\)](#) work the evolution of the system was vastly different. The systems final properties are therefore potentially less diagnostic of the physics involved in their growth than is the expression of a planet’s accretion profile in geochemical data. Rather, an approach that

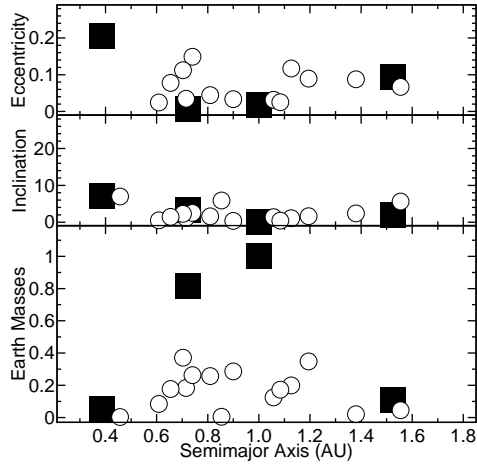


Fig. 10.— The final planets, after 115Myr of evolution, for  $R_{\text{init}} = 30$  km and no gas affects. Plotted are the (top) eccentricity, (middle) inclination in degrees and (bottom) mass as a function of semimajor axis. The large black squares are the values for Mercury, Venus, Earth and Mars, while the open circles are the simulation outcomes.

considers the constraints on growth timescales and also the compositional and internal evolution due to different growth profiles may be more important in assessing all of the important factors in Terrestrial Planet formation (Fischer et al. 2014; Dwyer et al. 2015; Carter et al. 2015).

Generally, a Mars-analog in these simulations accumulates most of its mass rapidly through the accretion of planetesimals, avoids late embryo-embryo collisions and its orbit diffuses outward from  $\sim 1$  au to its final semimajor axis at  $\sim 1.5$  au. This growth profile for Mars-analogs is not too different than that found in Hansen (2009), where Mars-analogs are scattered out and avoid further embryo-embryo accretion events after a few million years. The differences in these two evolutionary paths would lie primarily in the accretion profiles of Earth and Venus-analogs that alternately have long quiescent periods of accretion compared to somewhat regular embryo accretion events found in more classical models. In this way the systems in this work evolve similarly to that found in Levison et al. (2015) - whereby that work forms  $\sim 15$  planetary embryos between 0.7-1.5 au. This system of embryos is built rapidly and are stable for  $\sim 10$  Myr before embryo-embryo collisions begin.

Finally, this work was primarily an exploration of the dynamics of these systems as they grow from planetesimal to planets with and without the affects of a gaseous nebula. These tests were ideal first test cases for LIPAD as the small annulus required less total  $N$  than will the upcoming full-disk terrestrial planet simulations using the same code. However, the work found that for this test case that the collisional aspects of the code are much less important than is the total impact caused by the presence and lasting nature of the gaseous solar nebula. Upcoming work will expand on this work using similar techniques to study growth in a full-disk (0.7–3.0 au) and scenarios including giant planet migration.

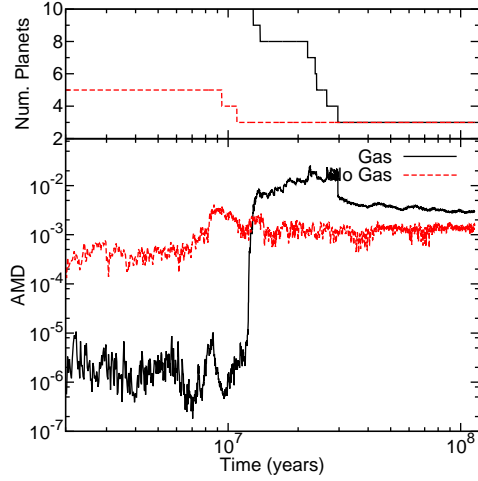


Fig. 11.— The (top) number of planets and (bottom) AMD plotted as a function of time for one case with gas (solid black line) and for a case with no gas (dashed red line).

## 5. Acknowledgements

The participation of KJW and HL was supported by NASA's SSERVI program (Institute of the Science of Exploration Targets) through institute grant number NNA14AB03A. This work used the Extreme Science and Engineering Discovery Environment (XSEDE), which is supported by National Science Foundation grant number ACI-1053575.

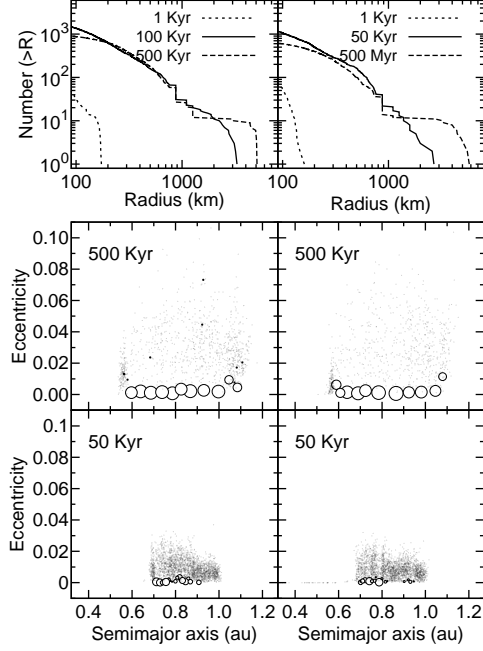


Fig. 12.— Evolution of two simulations, the left column are two panels showing the growth and evolution of the size frequency distribution without fragmentation, while the right panels include fragmentation.

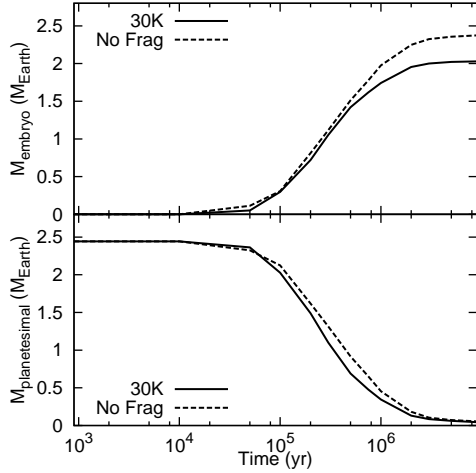


Fig. 13.— Evolution of two simulations, the top shows the growth of embryo mass over time and the bottom the total planetesimal mass over time for the nominal simulation with  $R_{\text{init}} = 30$  km and the case with no fragmentation.

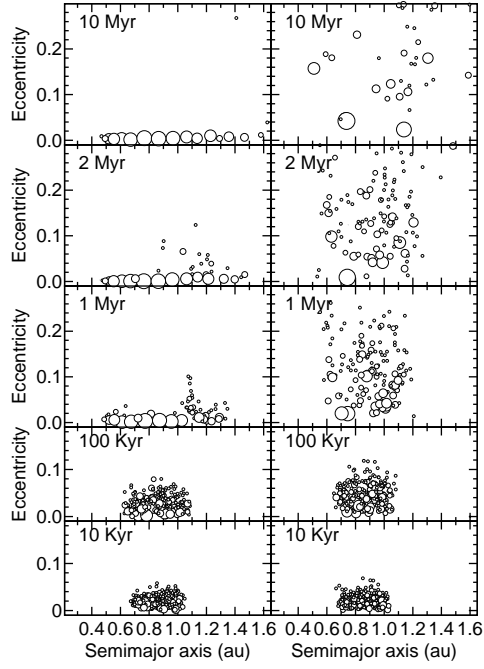


Fig. 14.— Comparing initial conditions from Hansen (2009) with and without a gas disk (left and right respectively).

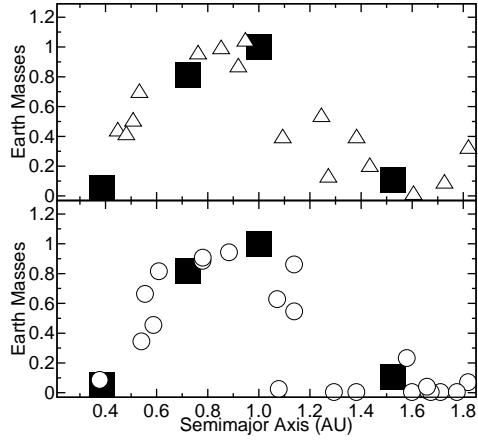


Fig. 15.— The top pane (open triangles) shows the orbital element distribution of planets using the Hansen 400 embryos initial conditions simulated in LIPAD with a gas-disk that dissipates on a 2-Myr timescale. The bottom pane (open circles) shows the same set of simulations run with no gas disk, to more directly reproduce the simulations of Hansen (2009).

## REFERENCES

- Carter, P. J., Leinhardt, Z. M., Elliott, T., Walter, M. J., & Stewart, S. T. 2015, eprint arXiv, 1509, 7504
- Chambers, J. E. 2001, *Icarus*, 152, 205, (c) 2001: Academic Press
- . 2013, *Icarus*, 224, 43, (c) 2013 Elsevier Inc.
- Dauphas, N., & Pourmand, A. 2011, *Nature*, 473, 489, (c) 2011: Nature
- Duncan, M. J., Levison, H. F., & Lee, M. H. 1998, *The Astronomical Journal*, 116, 2067, (c) 1998: The American Astronomical Society
- Dwyer, C. A., Nimmo, F., & Chambers, J. E. 2015, *Icarus*, 245, 145
- Fischer, R. A., Ciesla, F., & Campbell, A. J. 2014, American Geophysical Union, 44
- Hansen, B. M. S. 2009, *The Astrophysical Journal*, 703, 1131
- Ida, S., & Makino, J. 1993, *Icarus*, 106, 210
- Iwasaki, K., Emori, H., Tanaka, H., & Nakazawa, K. 2001, in *Bulletin of the American Astronomical Society*, Vol. 33, AAS/Division for Planetary Sciences Meeting Abstracts #33, 1060
- Izidoro, A., Haghighipour, N., Winter, O. C., & Tsuchida, M. 2014, *The Astrophysical Journal*, 782, 31
- Jacobson, S. A., & Morbidelli, A. 2014, *Phil. Trans. R. Soc. A*, 372, 0174
- Jin, L., Arnett, W. D., Sui, N., & Wang, X. 2008, *The Astrophysical Journal*, 674, L105
- Kenyon, S., & Bromley, B. 2006, *The Astronomical Journal*
- Kleine, T., Mezger, K., Palme, H., & Münker, C. 2004, *Earth and Planetary Science Letters*, 228, 109
- Kleine, T., Touboul, M., Bourdon, B., et al. 2009, *Geochimica et Cosmochimica Acta*, 73, 5150
- Kokubo, E., & Genda, H. 2010, arXiv, astro-ph.EP, 1003.4384v1, 21 pages, 3 figures, 2 tables, ApJL in press
- Kokubo, E., & Ida, S. 1998, *Icarus*, 131, 171
- Kominami, J., & Ida, S. 2002, *Icarus*, 157, 43
- Leinhardt, Z. M., Richardson, D. C., Lufkin, G., & Haseltine, J. 2009, *Monthly Notices of the Royal Astronomical Society*, 396, 718



- Levison, H., Duncan, M., & Thommes, E. 2012, *The Astronomical Journal*
- Levison, H. F., Kretke, K., Walsh, K. J., & Bottke, W. F. 2015, *Proceedings of the National Academy of Sciences*, 112, 46
- Morbidelli, A., Lunine, J., O’Brien, D., Raymond, S., & Walsh, K. 2012, *Annu. Rev. Earth. Planet. Sci.*, 40, 251, d
- Morishima, R. 2015, arXiv, astro-ph.EP, 1508.07377v1
- Nimmo, F., & Kleine, T. 2007, *Icarus*, 191, 497
- O’Brien, D. P., Morbidelli, A., & Levison, H. F. 2006, *Icarus*, 184, 39
- O’Brien, D. P., Walsh, K. J., Morbidelli, A., Raymond, S. N., & Mandell, A. M. 2014, *Icarus*, 239, 74, (c) 2014 The Authors
- Ormel, C., & Dullemond... , C. 2010, *The Astrophysical Journal* ...
- Raymond, S. N., O’Brien, D. P., Morbidelli, A., & Kaib, N. A. 2009, *Icarus*, 203, 644
- Thommes, E. W., Duncan, M. J., & Levison, H. F. 2003, *Icarus*, 161, 431
- Walsh, K., Morbidelli, A., Raymond, S., O’Brien, D., & Mandell, A. 2011, *Nature*, 475, 206
- Wisdom, J., & Holman, M. 1991, *Astronomical Journal* (ISSN 0004-6256), 102, 1528